Interaction of Graphene and Arenes with Noble Metals

ARTICLE *in* THE JOURNAL OF PHYSICAL CHEMISTRY C · JUNE 2012

Impact Factor: 4.77 · DOI: 10.1021/jp3030733

THE JOURNAL OF PHYSICAL CHEMISTRY C

Article

pubs.acs.org/JPCC

Interaction of Graphene and Arenes with Noble Metals

Jaroslav Granatier,[†,§] Petr Lazar,[‡,§] Robert Prucek,[‡] Klára Šafářová,[‡] Radek Zbořil,[‡] Michal Otyepka,*[,‡] and Pavel Hobza*[,†,‡]

[†]Institute of Organic Chemistry and Biochemistry, Academy of Sciences of the Czech Republic, Flemingovo nam. 2, 166 10 Prague 6, Czech Republic

[‡]Regional Centre of Advanced Technologies and Materials, Department of Physical Chemistry, Faculty of Science, Palacky University, 771 46 Olomouc, Czech Republic

ABSTRACT: The structure, binding energies, and nature of bonding of coronene···X_2 and coronene···X_4 (X = Pd, Ag, Au) complexes were investigated at the MP2 and DFT levels. The reliability of the MP2 calculations was confirmed for benzene···X_2 (X = Pd, Ag, Au) complexes by comparison with benchmark values obtained at the CCSD(T) level. Both calculations demonstrated that the bonds formed by palladium complexes with the surface are considerably stronger than those of gold, which in turn are stronger than silver complexes. The silver and gold clusters bind to carbon surfaces through dispersion and charge-transfer interactions, whereas the palladium clusters are bound by dative bonds. MP2 calculations on coronene···X complexes indicated that the binding energies of Pd, Ag, and Au clusters increase linearly with the number of metal atoms. The same trend was observed for graphene···X complexes, except graphene···Pd_4. M06-2X calculations indicated that binding energies of coronene···X complexes in water were only slightly smaller than those in vacuum. On the basis of the MP2 calculations, we conclude that the stability of metal clusters (up to tetramers) on coronene increases as follows: Pd ≫ Au > Ag. This finding was supported by our scanning electron microscopy observations of metal nanoparticles (~20 nm) on graphene composites.

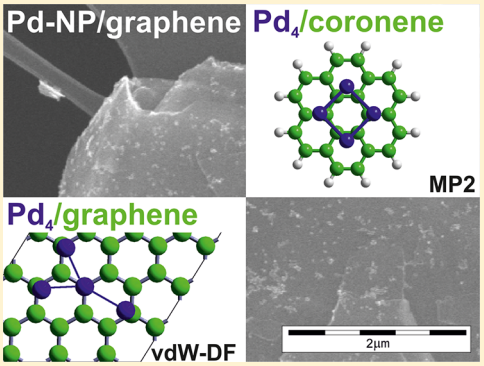

INTRODUCTION

Graphene is a single atom thick two-dimensional sheet of sp^2-bonded carbon atoms packed into a honeycomb lattice.[1,2] It is a zero-gap semiconductor with a unique electronic structure, in which electrons obey linear dispersion, mimicking massless relativistic particles. Its two-dimensional crystal structure generates many interesting properties, such as quantum Hall effects,[3,4] ballistic quantum properties,[2,5] absence of localization, etc. This makes graphene and graphene-containing hybrid materials attractive for electronics, spintronics, optics, catalysis, and sensing applications.[6]

Interaction of solid metals, metal clusters, and nanoparticles with graphene has been observed in many hybrid systems with a broad range of potential applications, including sensing, hydrogen storage, catalysis, and nano(opto)electronics.[7−14] The extensive diversity of metal atoms, size of their clusters, and size and shape of their nanoparticles offer enormous scope for the controlled modification of graphene for specific applications. An understanding of the metal−graphene interaction, and particularly the nature of the interaction, is useful for the rational development of hybrid materials with selected properties. Therefore, the interaction of graphene with metal substrates, and their electronic and structural properties as the stabilities, distances, nature of binding, charge transfer between graphene and metallic surface, etc., have been studied theoretically and experimentally.[15−17]

The interaction of transition metal atoms and their clusters with graphene can involve a large component of dispersion interactions, stemming from nonlocal electron−electron correlation. Theoretical studies of graphene and its complexes with transition elements have often involved density functional theory (DFT) utilizing local density approximation (LDA)[18−20] or generalized-gradient approximation (GGA).[21−25] However, these DFT approaches are based on a local approximation for the exchange-correlation functional, which cannot accurately represent the dispersion energy. Several techniques have been developed to improve these DFT approaches, which take account of dispersion interactions either explicitly or implicitly.[26,27] The van der Waals density functional (vdW-DF) method and its variations seem to be especially promising for describing the interaction of graphene with metals.[28,29] On the other hand, quantum chemistry methods can accurately and consistently describe the nonlocal electron correlations. In this respect, coupled cluster method covering single and double electron excitations iteratively and triple electron excitations perturbatively (CCSD(T))[30−32] accounts for a large proportion of electron correlations (when applied with a large basis set). CCSD(T) represents a gold standard in today's computational chemistry and provides a sufficiently accurate description of

Received: March 30, 2012
Revised: May 11, 2012
Published: June 8, 2012

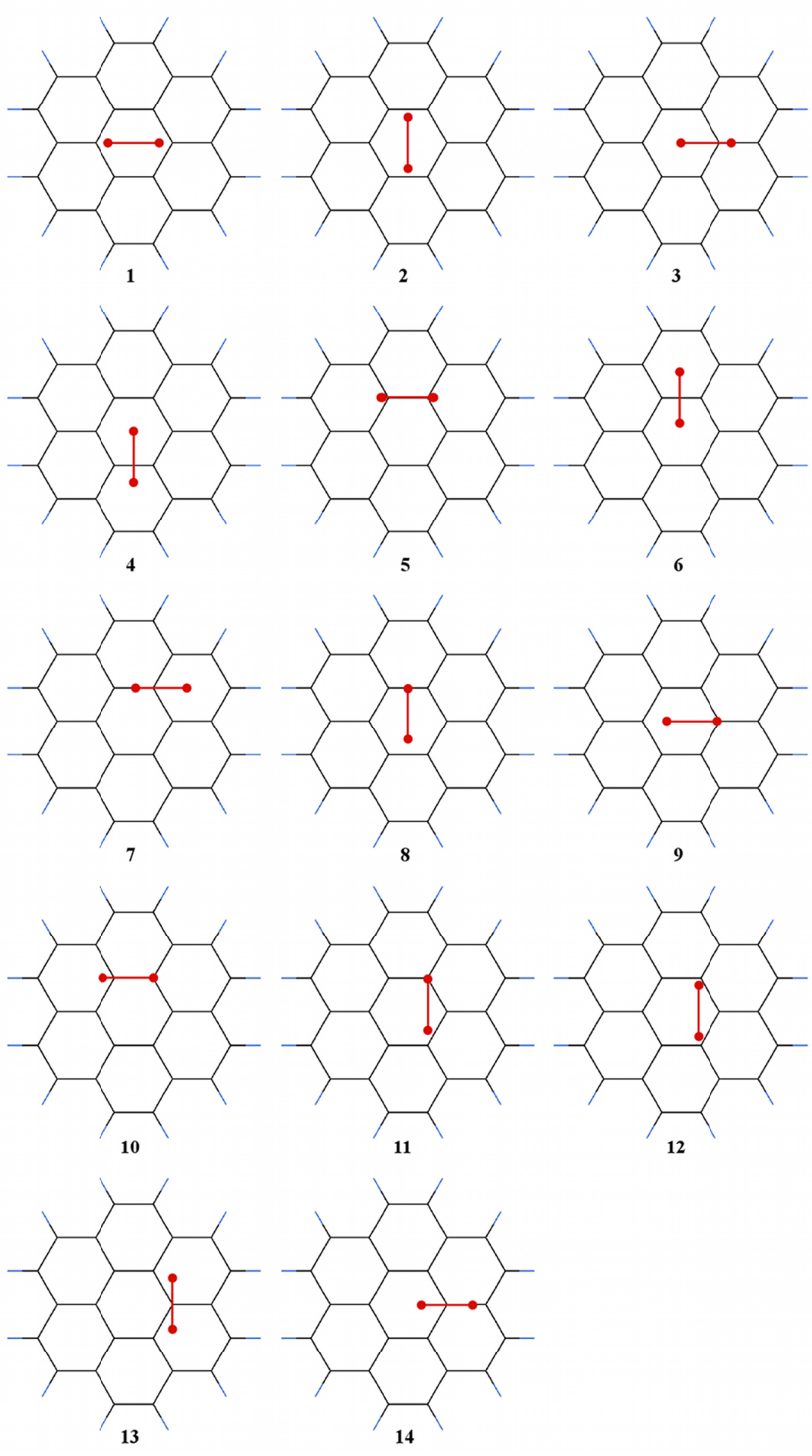

Figure 1. The 14 studied structures of coronene···X_2 complexes.

various types of noncovalent complexes. When combined with atomic orbital basis set large enough, or even better extrapolated to a complete basis set limit (CBS), the accuracy of the method approaches subchemical (~0.1 kcal/mol) accuracy, at least for noncovalent complexes of organic molecules. However, it should be noted that the accuracy of CCSD(T) for compounds with transition metals is expected to be slightly lower.[33,34] CCSD(T)/CBS calculations are, in general, computationally highly demanding and can thus only be performed for small complexes up to about ~30 atoms. For calculations of more extended complexes, less-demanding methods, such as MP2 or DFT, which take account of the dispersion energy, must be utilized.

In previous work, we focused on the nature of binding of single palladium, silver, and gold atoms on arene rings, represented by benzene, coronene, and periodic graphene surfaces.[29] We concluded that the bonds formed between the metal atoms and carbon surface were of a different nature as follows; silver atoms predominantly bound through dispersion interactions, whereas the binding of gold complexes was, beside

dx.doi.org/10.1021/jp3030733 | J. Phys. Chem. C 2012, 116, 14151−14162

dispersion, mediated by charge transfer from the carbon surface to the metal atom. However, in the latter interaction, the degree of charge transfer varied for different adsorption sites; it was significant for bridge (gold atom above a C−C bond) and top (gold atom directly above carbon atom) structures but not for hollow sites (gold atoms above the center of a benzene ring). The adsorption of Pd atoms was quite different because bonding to the carbon surface was partially realized by a dative bond. Our results also demonstrated that plane-wave DFT yields binding energies and distances that agree very well with reference CCSD(T) values when augmented with a nonlocal van der Waals correction (vdW-DF) and one-quarter of the exact exchange (EE) (this method is hereafter referred to as EE +vdW).

In the present work, we studied the adsorption of larger metal models (X_2 and X_4) on aromatic carbon surfaces. Our ultimate goal was to investigate interactions between aromatic carbon surfaces and metal dimers or tetramers as representative models of metal surfaces. In this respect, we only considered planar interactions with dimers and tetramers and not, for example, perpendicular interactions of metal dimers with carbon surfaces. Similarly, we only considered singlet states of the metal models, although we are aware that, in case of gold and silver tetramers, higher multiplicity states are more stable than the singlet states.[35] Specifically, we considered the adsorption of palladium, silver, and gold dimers and tetramers in a planar conformation on coronene and graphene surfaces. The systems investigated were too large for application of the CCSD(T) method. Therefore, we performed the calculations at the MP2[36] and DFT-D[37−39] levels (for coronene complexes) and EE+vdW level (for graphene complexes). In our previous study, we showed that the MP2 method combined with the ANO-RCC-VDZP basis set provides binding energies for all adatoms and structures that are closely comparable with CCSD(T)/ANO-RCC-VTZP values. In the first step of the present study, we verified this finding by performing CCSD(T) and MP2 calculations for benzene···X_2 (X = Pd, Ag, Au) complexes. In the second step, we focused on evaluating the gas-phase binding energies of metal dimers and tetramers on coronene and graphene surfaces using the MP2, DFT-D, and EE+vdW methods. In the third step, we investigated the binding of the metal clusters to coronene in the presence of water. In this case, only the M06-2X method accommodating the dispersion energy was considered. Finally, we prepared metal nanoparticles (∼20 ns) on composite graphene surfaces and observed them by scanning electron microscopy (SEM) to estimate their affinities to graphene.

COMPUTATIONAL DETAILS

All calculations were performed with an ANO-RCC basis set optimized for relativistic calculations.[40,41] This basis contains polarization and diffusion functions and is thus useful for calculations of noncovalent complexes. Relativistic effects for all complexes containing heavy metals were taken into account by using the scalar one-component second-order Douglas−Kroll−Hess approximation.[42,43]

Structure, interaction energies, and the nature of bonding of coronene···X_2 and coronene···X_4 complexes were studied at wave function theory (WFT) with second-order Möller−Plesset perturbation (MP2)[36] level together with hybrid functional M06-2X[37−39] utilizing an ANO-RCC-VDZP basis set. The MP2/ANO-RCC-VDZP results for two structures of benzene···X_2 (X = Pd, Ag, and Au) complexes were compared to benchmark values calculated by the CCSD(T)/ANO-RCC-VTZP method. All carbon electrons except the 1s electrons as well as the $4p^6 4d^{10}$ shells of palladium, $4p^6 4d^{10} 5s^1$ shells of silver, and $5p^6 5d^{10} 6s^1$ shells of gold were correlated. All of the WFT interaction energies were corrected for the basis sets superposition error (BSSE) by using the counterpoise correction.[44]

The M06-2X calculations were performed on all electron ANO-RCC-VDZP and pseudopotential lanl2dz[45,46] basis sets. Coronene···X_2 and coronene···X_4 complexes in vacuum and water were treated at the M06-2X/lanl2dz level. The continuum SMD solvation model[47] was used for calculations in water.

The MP2/ANO-RCC-VDZP and M06-2X/ANO-RCC-VDZP interaction energies were calculated in parallel mode by using the Cholesky decomposition[48] with a moderately accurate configuration of decomposition (threshold 10^{-6} hartree). The former calculations for coronene···X_4 complexes were, however, performed with a higher threshold of 10^{-8} hartree because the standard threshold calculations gave barely interpretable results. Calculations were performed using the MOLCAS[49] and GAUSSIAN 09[50] program packages. The M06-2X and MP2 interaction energy curves were interpolated by a sixth-order polynomial.

The X_2 and X_4 (X = Pd, Ag, and Au) systems were optimized at the DKH-CCSD(T)/ANO-RCC-VTZP level in D_{2h} symmetry; for the latter systems, planar square and orthorhombic structures were considered. The structure of coronene was taken from our previous study and was determined by MP2/cc-pVTZ optimization in C_{2v} symmetry. Structures of all subsystems (X_2, X_4, and coronene) were kept frozen in all subsequent DFT and WFT optimizations.

Structures of coronene···X_2 complexes were generated with the aim of including all possible types of adsorption positions and are shown in Figure 1. Specifically, structures 1 and 2 correspond to hollow(coronene)···bridge(metal dimer) interactions. However, because the width of carbon ring is similar to the distance between metal atoms, these structures approximately describe the double top···top and bridge···top interactions. Structures 3 and 4 correspond to hollow···top type interactions, whereas structure 5 and 6 describe bridge···bridge interactions. In structures 7 and 8, the metallic atom is bound to a bridge site of coronene. In structures 9, 10, and 11, the metallic atom is bound to a top position of the coronene central ring. Structure 12 is a special structure reflecting a double top···top interaction (the distances between the carbon atoms and metallic atoms were similar). Structures 13 and 14 describe top···bridge interactions. All four structures of the coronene···X_4 complexes are characterized by C_{2v} symmetry and are displayed in Figure 2.

Plane-wave DFT calculations were performed to model the graphene surface, using the Vienna Ab initio Simulation Package (VASP), which makes use of the projector-augmented wave (PAW) construction for the pseudopotential.[51,52] The generalized gradient approximation of Perdew−Burke−Ernzerhof (PBE)[53] method was used to parametrize the exchange-correlation function. The structural parameters of graphene were relaxed by minimizing the forces acting on the atoms using a conjugate-gradient algorithm. The energy cutoff for the plane-wave expansion of the eigenfunctions was set to 500 eV. The graphene sheet was modeled using a 4 × 4 supercell (each supercell contained 32 carbon atoms) with a calculated C−C bond length of 1.44 Å. The repeated sheets were separated

dx.doi.org/10.1021/jp3030733 | J. Phys. Chem. C 2012, 116, 14151−14162

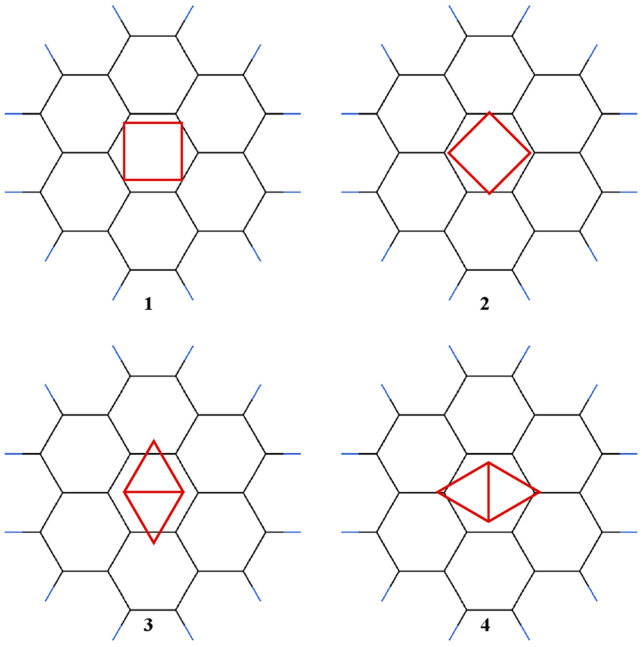

Figure 2. The studied square (1 and 2) and orthorhombic (3 and 4) structures of X_4 adsorbed on coronene.

from each other by 22 Å of vacuum. The shortest in-plane distance between metal atoms was 7 Å. We performed a test calculation with a large 8 × 8 supercell (containing 128 atoms). The results showed that the total energies of the 4 × 4 supercell had already converged, and there was no significant in-plane interaction of repeated dimers and tetramers. A gamma-centered 5 × 5 × 1 k-point mesh was found to give converged total energies and was consequently used for the Brillouin-zone integration. Spin polarization was taken into account in all calculations. Long-range van der Waals (dispersion) interactions, which are absent in standard DFT, were included by means of the van der Waals density functional (vdW-DF)[54] for PBE-optimized geometries.

The core of the vdW-DF method is a fully nonlocal expression for the correlation energy, E_{nl}^{c}, which takes the following form:

$$E_{nl}^{c} = \int dr^3 dr'^3 n(r)\Phi(r, r')n(r') \quad (1)$$

Here, $n(r)$ is the electron density obtained from a standard DFT calculation, and the kernel $\Phi(r, r')$ is a function that depends on $r-r'$ and the magnitudes and gradients of the electron densities at the points r and r'. We used the JuNoLo program to evaluate the vdW term, with PBE electron densities serving as inputs.[55] The total energy was then calculated by replacing PBE correlation energy E_c^{PBE} with its nonlocal counterpart E_c^{nl}:

$$E_{tot}^{nl} = E_{tot}^{DFT} - E_c^{PBE} - E_x^{PBE} + (E_x^{PBE} + E_c^{LDA} - E_c^{nl}) \quad (2)$$

We refer to this method as PBE+vdW. The PBE exchange energies E_x^{PBE} are written out explicitly to emphasize that the PBE exchange energy inside the parentheses could in principle be replaced by the exchange energy obtained by some other formulation. In our previous paper,[29] we demonstrated that replacing one-quarter of E_x^{PBE} with the exact Hartree–Fock exchange energy, E_x^{HF}, results in very close agreement with benchmark CCSD(T) calculations. Thus, we also adopted this approach (denoted as EE+vdW) to study noble metal clusters.

Materials. Silver nitrate (99.9%, Sigma-Aldrich), ammonia (28% w/w aqueous solution, p.a., Sigma-Aldrich), sodium hydroxide (p.a., Lachema), D(+)-maltose monohydrate (p.a. purity, Sigma-Aldrich), $HAuCl_4 \cdot 3H_2O$ (99.99%, Sigma-Aldrich), K_2PdCl_4 (99.99%, Sigma-Aldrich), ascorbic acid (p.a., Lachema), and graphene powder (Durham Graphene Science Ltd.; few-layered graphene sheets manufactured using a CVD-based process) were used without further purification.

Synthesis of Metal Nanoparticles. Silver nanoparticles were synthesized by reduction of the complex $[Ag(NH_3)_2]^+$ cation with D-maltose.[56] The final concentrations of the reaction components were 10^{-3} and 10^{-2} M for $AgNO_3$ and D-maltose, respectively. The final concentration of ammonia used was 5×10^{-3} M. Sodium hydroxide solution was added to the reaction system to adjust the pH to 11.5. The average particle size of Ag nanoparticles was 28 nm according to dynamic light scattering (DLS) measurements.

Au and Pd NP were synthesized by a modified method using ascorbic acid as reductant.[57] Gold nanoparticles were prepared by reduction of $HAuCl_4$ with ascorbic acid. The pH of the reaction mixture was adjusted to 4.5, and the average particle size was 25 nm as determined by DLS. Palladium nanoparticles were synthesized by reduction of K_2PdCl_4 with ascorbic acid. The pH of the reaction mixture was adjusted using aqueous solution of NaOH to 9.0, and the average particle size was 22 nm by DLS. All syntheses were performed at laboratory temperature (20 °C), and following separation, all noble metal nanoparticles were washed several times with deionized water.

Synthesis of Metal Nanoparticles–Graphene Composites. For the qualitative evaluation of the interaction of noble metal nanoparticles with graphene, 100 μL of aqueous dispersions containing noble metal nanoparticles (20 mg/L) was added to 200 μL of colloidal dispersions of graphene in deionized water (5 mg/L). After being shaken (30 min) in a glovebox, a drop of the colloidal mixture was dispensed onto a carbon-coated copper grid and evaporated at room temperature. The grid was subsequently transferred to a SEM to monitor the affinity and interaction of noble metals with graphene sheets.

Characterization Techniques. The average size of noble metal nanoparticles was evaluated by a dynamic light-scattering method (Zetasizer Nano ZS, Malvern). Scanning electron micrographs were acquired using a field-emission SU6600 (Hitachi) SEM operating at 15 kV.

RESULTS AND DISCUSSION

X_2. The X_2 dimers were optimized at the CCSD(T)/ANO-RCC-VDZP level (spin–orbit effects were neglected), and equilibrium geometries, binding energies (the ZPVE energies were not included), and their properties are presented in Table 1. The binding energies of Ag_2 and Au_2 in their ground singlet states are 34.40 and 48.04 kcal/mol, respectively. The ground state of palladium dimer has not been uniquely determined. While single determinant methods are sufficient for describing the singlet state of Pd_2, methods based on a multireference approach are required to calculate its triplet state. At the MRSDCI/RCI level, the ground state of Pd_2 is predicted to be a triplet state.[58] However, the singlet state is the ground state at CASPT2/MP2, MP3, and MP4 levels.[59] Because of high excitation amplitudes, the CCSD(T) approach is not applicable for calculations of the triplet state of Pd_2. The CCSD(T)

dx.doi.org/10.1021/jp3030733 | J. Phys. Chem. C 2012, 116, 14151–14162

Table 1. Structural and Electronic Parameters of Pd, Ag, and Au Atoms and Their Dimers[a]

	Pd		Ag		Au	
	atom	dimer	atom	dimer	atom	dimer
E [kcal/mol]		6.66		34.40		48.04
R_e [Å]		2.77		2.56		2.51
IP_{vert} [eV]	8.35	6.33	7.52	7.62	9.12	9.34
EA_{vert} [eV]	0.36	1.27	1.16	0.88	2.17	1.76
α [au]	19.18	35.27	46.29	51.12	33.41	39.48

[a]All of the data have been obtained at the DKH-CCSD(T)/ANO-RCC-VTZP level with inclusion of relativistic effects. The evaluation of the polarizabilities was accomplished using the numerical finite field perturbation approach with external field 0.001.[61] The binding energy of dimers has been treated by BSSE correction.

binding energy of the singlet state of Pd_2 is 6.66 kcal/mol. The singlet Pd_2 state was considered to facilitate the comparison with singlet Au and Ag dimers included in this study.

This difference in binding energies of X_2 (X = Pd, Ag, Au) can be easily explained on the basis of occupancies of bonding and antibonding orbitals of the respective dimers. The valence d-orbitals of the palladium atom are fully occupied. Consequently, all bonding and antibonding orbitals in the dimer are fully occupied, and bonding between palladium atoms is weak. This is also reflected by the zero-bond order of Pd_2. Silver and gold atoms in the respective dimers are bonded by a σ-bond, which is formed by the overlap of singly occupied valence s-orbitals. The binding in these dimers is thus strongly covalent. The ionization potentials (IP) and electron affinities (EA) of the respective atoms and dimers also exhibit distinct differences. In the case of palladium, the IP and EA of the atom are larger and smaller, respectively, than the corresponding values of dimers. In contrast, silver and gold dimers have larger IP and smaller EA than isolated metal atoms. Investigating the electronic structure of the Ag_2 and Au_2 dimers, we found that the highest occupied orbital is a bonding σ-orbital and the lowest unoccupied orbital is an antibonding σ-orbital. In contrast, the highest occupied orbital in the palladium dimer is antibonding, while the lowest unoccupied orbital is bonding. Therefore, the addition or removal of electrons decreases the bond order as well as the binding energy in silver and gold dimers but increases the binding energy and bond order in palladium dimers. The dipole polarizabilities of Ag_2 and Au_2 are slightly different than atomic values, whereas the polarizability of Pd_2 is about 45% larger than that of the Pd atom.

On the basis of the calculated IP and EA of metal dimers, we can make initial predictions regarding the nature of binding of these dimers to carbon surfaces. We expect that the palladium dimer will bind to the carbon surface by a dative bond. The dative bond in Pd_2···coronene should be stronger than that in Pd···coronene due to the higher electron affinity and lower ionization potential of Pd_2. The lower EA of silver and gold dimers as compared to the respective atoms is expected to reduce the charge transfer from the carbon surface to metal dimers. However, the higher polarizability and ionization potential of the latter dimers should lead to stronger dispersion interactions.

X_2···Benzene. The CCSD(T)/ANO-RCC-VTZP and MP2/ANO-RCC-VDZP binding energies and intermolecular distances for benzene···X_2 (X = Pd, Ag, Au) complexes are collected in Table 2. The first and second structures investigated possess C_{2v} symmetry and are thus analogous to

Table 2. Binding Energies (ΔE in kcal/mol) and Bond Lengths (R in Å) for Two Different Structures of Benzene···X_2 (X_2 = Pd, Ag, Au) Complexes Evaluated at the DKH-CCSD(T)/ANO-RCC-VTZP and DK-MP2/ANO-RCC-VDZP Levels[a]

	benzene···Pd_2		benzene···Ag_2		benzene···Au_2	
	1	2	1	2	1	2
CCSD(T)/ANO-RCC-VTZP						
ΔE	34.00	35.94	2.42	2.41	3.65	3.64
R	2.16	2.13	3.45	3.45	3.28	3.29
MP2/ANO-RCC-VDZP						
ΔE	34.61	36.96	2.82	2.82	5.67	5.65
R	2.13	2.09	3.44	3.44	3.12	3.12

[a]The studied structures correspond to 1 and 2 depicted in Figure 1. All binding energies are BSSE corrected.

structures 1 and 2 for coronene···X_2 (cf., Figure 1). The MP2 results for benzene···Pd_2 complexes are reasonably similar to those calculated at the CCSD(T)/ANO-RCC-VTZP level. In the case of palladium, the MP2 method slightly overestimates the binding energies (by about 0.6 and 1.1 kcal/mol for structures 1 and 2, respectively) and slightly underestimates intermolecular distances (by about 0.04 Å). In the case of silver and gold complexes, the differences are larger; MP2 systematically overestimates the binding by 17% and 55%, respectively. Despite the fact that the MP2 method overestimates the binding energy, especially for the benzene···Au_2 complexes, it is a useful approach to compare with the CCSD(T) method for describing the nature of bonding in these complexes.

X_2···Coronene. Interaction energies and geometries of the coronene···X_2 complexes calculated at the MP2 and M06-2X levels are collected in Tables 3−5. Table 4 shows that the MP2 binding energies and intermolecular distances for various structures of the coronene···Ag_2 complexes are similar and lie in the interval 8.4 ± 0.5 kcal/mol and 3.22 ± 0.04 Å, respectively. The preferred adsorption site corresponds to a double top···top or bridge···top interaction (structures 1, 2, 8, 9, 11, and 12). The largest binding energies are 8.9 kcal/mol (structures 1, 2, 8, 9) followed by 8.6 kcal/mol (structures 11 and 12). The other structures characterized by single top···top or bridge···top interactions are less stable. The M06-2X method slightly underestimates the stabilization energies by about 0.8−1.5 or 1.3−2.0 kcal/mol when the pseudopotential lanl2dz or all electron ANO-RCC-VDZP basis sets are utilized, respectively. The M06-2X intermolecular distances closely agree with the MP2 distances.

The interaction of Ag_2 with coronene is governed by dispersion and, to a lesser extent, charge-transfer energies. The lower electron affinity of the silver dimer in comparison with that of atomic silver implies there is less charge transfer from coronene to the silver dimer. In contrast, the higher polarizability and ionization potential of the silver dimer as compared to a silver atom indicates an increased dispersion energy in the adsorption of silver dimer at the coronene surface. The MP2 charge analysis indeed suggests that there is a smaller charge transfer from coronene to silver atoms in the dimer (the charge on each atom of the dimer was predicted to be about −0.042) in comparison with charge transfer in coronene···Ag complexes (−0.052).[29] The preferred adsorption position of Ag_2 on a coronene surface corresponds to structures

dx.doi.org/10.1021/jp3030733 | J. Phys. Chem. C 2012, 116, 14151−14162

Table 3. Binding Energies (ΔE in kcal/mol) and Intermolecular Distances (R in Å) for All Structures of Coronene···Pd_2 Complexes (cf., Figure 1) Calculated at the DKH-MP2/ANO-RCC-VDZP, DKH-M06-2X/ANO-RCC-VDZP, and M06-2X/lanl2dz Levels[a]

	structure													
	1	2	3	4	5	6	7	8	9	10	11	12	13	14
MP2/ANO-RCC-VDZP														
ΔE	35.72	33.89	35.85	33.04	33.10	31.22	39.19	33.68	35.69	34.07	36.66	36.68	34.51	35.98
R	2.12	2.10	2.07	2.00	2.07	2.00	2.06	2.10	2.12	2.08	2.11	2.11	2.07	2.07
M06-2X/ANO-RCC-VDZP														
ΔE	22.24	21.15	22.20	20.71	20.24	20.18	23.68	21.10	22.27	21.52	22.47	22.25	21.37	22.20
R	2.43	2.44	2.41	2.45	2.44	2.47	2.38	2.44	2.42	2.43	2.41	2.41	2.43	2.41
M06-2X/lanl2dz (vacuum)														
ΔE	23.69	23.23	24.10	23.10	22.56	22.70	25.00	23.18	23.81	23.44	23.93	23.96	23.57	24.18
R	2.54	2.54	2.49	2.51	2.54	2.52	2.48	2.54	2.53	2.51	2.52	2.52	2.52	2.49
M06-2X/lanl2dz (water)														
ΔE	24.22	23.53	24.22	22.62	22.49	22.20	25.20	23.43	24.36	23.50	24.57	24.54	23.64	24.34
R	2.51	2.53	2.48	2.51	2.54	2.53	2.47	2.53	2.51	2.51	2.5	2.5	2.51	2.48

[a]The MP2 binding energies are corrected for the BSSE correction. The M06-2X/lanl2dz data were calculated for vacuum and aqueous environments.

Table 4. Binding Energies (ΔE in kcal/mol) and Bond Lengths (R in Å) for Structures of Coronene···Ag_2 Complexes (cf., Figure 1) Calculated at the DKH-MP2/ANO-RCC-VDZP, DKH-M06-2X/ANO-RCC-VDZP, and M06-2X/lanl2dz Levels[a]

	structure													
	1	2	3	4	5	6	7	8	9	10	11	12	13	14
MP2/ANO-RCC-VDZP														
ΔE	8.90	8.88	8.15	8.24	8.20	8.30	7.97	8.85	8.87	8.17	8.63	8.61	8.18	7.99
R	3.20	3.22	3.26	3.24	3.26	3.25	3.23	3.21	3.18	3.23	3.24	3.24	3.22	3.25
M06-2X/ANO-RCC-VDZP														
ΔE	7.08	6.96	6.81	6.98	6.73	6.96	6.70	6.98	7.00	6.70	6.88	7.09	6.90	6.71
R	3.26	3.28	3.27	3.27	3.26	3.26	3.23	3.27	3.23	3.26	3.23	3.25	3.23	3.28
M06-2X/lanl2dz (vacuum)														
ΔE	7.46	7.45	7.12	7.34	7.22	7.36	7.12	7.45	7.46	7.26	7.37	7.37	7.39	7.00
R	3.28	3.28	3.28	3.27	3.29	3.27	3.27	3.28	3.28	3.28	3.28	3.28	3.27	3.29
M06-2X/lanl2dz (water)														
ΔE	6.71	6.69	6.61	6.71	6.48	6.73	6.52	6.69	6.70	6.64	6.69	6.64	6.66	6.51
R	3.37	3.36	3.35	3.35	3.36	3.35	3.37	3.37	3.37	3.35	3.35	3.36	3.35	3.35

[a]The MP2 binding energies are corrected for the BSSE correction. The M06-2X/lanl2dz data were calculated for vacuum and aqueous environments.

Table 5. Binding Energies (ΔE in kcal/mol) and Bond Lengths (R in Å) for Structures of Coronene···Au_2 Complexes (cf., Figure 1) at the DKH-MP2/ANO-RCC-VDZP, DKH-M06-2X/ANO-RCC-VDZP, and M06-2X/lanl2dz Levels[a]

	structure													
	1	2	3	4	5	6	7	8	9	10	11	12	13	14
MP2/ANO-RCC-VDZP														
ΔE	12.98	12.73	12.05	12.28	11.64	12.35	11.95	12.75	12.94	11.86	12.52	12.52	12.00	11.77
R	3.02	3.05	3.07	3.06	3.11	3.05	3.04	3.05	3.03	3.09	3.04	3.04	3.07	3.07
M06-2X/ANO-RCC-VDZP														
ΔE	7.32	7.29	7.06	7.38	7.01	7.29	6.96	7.14	7.08	6.85	7.11	7.10	7.09	6.92
R	3.24	3.22	3.23	3.22	3.3	3.24	3.19	3.23	3.22	3.28	3.25	3.27	3.25	3.22
M06-2X/lanl2dz (vacuum)														
ΔE	9.06	9.00	8.76	9.10	8.61	9.11	8.83	9.00	9.06	8.80	8.92	8.91	9.02	8.54
R	3.24	3.24	3.23	3.21	3.26	3.21	3.23	3.24	3.23	3.25	3.25	3.24	3.23	3.24
M06-2X/lanl2dz (water)														
ΔE	8.70	8.65	8.70	8.88	8.29	8.90	8.58	8.65	8.70	8.56	8.64	8.58	8.70	8.52
R	3.35	3.34	3.33	3.32	3.36	3.32	3.34	3.34	3.34	3.37	3.35	3.35	3.33	3.33

[a]The MP2 binding energies are corrected for the BSSE correction. The M06-2X/lanl2dz data were calculated for vacuum and aqueous environments.

characterized by double charge transfer from coronene to the silver atoms.

The binding energies of coronene···Au_2 (Table 5) are, in comparison with coronene···Ag_2 complexes, larger and the

dx.doi.org/10.1021/jp3030733 | J. Phys. Chem. C 2012, 116, 14151−14162

Table 6. Binding Energies (ΔE in kcal/mol) and Bond Lengths (R in Å) for Structures of Coronene···X_4 (X = Pd, Ag, Au) Complexes (cf., Figure 2) at the DK-MP2/ANO-RCC-VDZP, DK-M06-2X/ANO-RCC-VDZP, and M06-2X/lanl2dz Levels[a]

	Pd_4···coronene				Ag_4···coronene				Au_4···coronene			
	1	2	3	4	1	2	3	4	1	2	3	4
MP2/ANO-RCC-VDZP												
ΔE	70.69	*71.82*	*39.03*	*44.63*	13.96	18.18	16.49	16.24	18.50	25.04	23.69	*23.31*
R	2.09	*2.08*	*2.09*	*2.08*	3.22	3.22	3.28	3.26	3.07	3.08	3.10	*3.12*
M06-2X/ANO-RCC-VDZP												
ΔE	45.46	45.46	16.79	16.44	14.35	14.47	12.76	12.42	12.91	13.13	13.38	12.79
R	2.52	2.52	2.99	3.00	3.38	3.33	3.34	3.39	3.26	3.29	3.31	3.30
M06-2X(vacuum)/lanl2dz												
ΔE	56.39	56.34	15.39	14.98	14.38	14.77	13.68	13.32	12.91	17.15	16.87	16.32
R	2.62	2.61	3.18	3.20	3.33	3.35	3.34	3.36	3.28	3.28	3.28	3.30
M06-2X(water)/lanl2dz												
ΔE	46.44	46.36	14.26	13.84	14.97	13.16	12.51	12.25	14.80	17.21	16.65	16.15
R	2.62	2.61	3.34	3.34	3.58	3.45	3.46	3.46	3.38	3.40	3.40	3.41

[a]The MP2 binding energies are corrected for the BSSE correction. The M06-2X/lanl2dz data were calculated for vacuum and aqueous environments.

intermolecular distances are smaller. MP2 binding energies are about 12.4 ± 0.6 kcal/mol (with the largest difference of 1.3 kcal/mol), and distances of Au_2 from the coronene surface are in the range 3.0−3.1 Å. The preferred adsorption sites are the same as those for coronene···Ag_2 complexes. Binding energies of the most stable structures (1 and 9) and the next highest (2, 8, 11, and 12) differed by less than 0.5 kcal/mol.

The M06-2X/ANO-RCC-VDZP stabilization energies are about 60% of the MP2 energies. Although the M06-2X/lanl2dz method provides a better estimate of the stabilization energies than does the M06-2X/ANO-RCC-VDZP method, the respective stabilization energies are still underestimated by about 3.0−3.9 kcal/mol. Further, the M06-2X intermolecular distances are about 0.2 Å longer than the MP2 bond lengths and are comparable to those in the coronene···Ag_2 complexes.

Analyzing the nature of stabilization in the coronene···Au_2 and coronene···Ag_2 complexes, we found marked similarities, especially in the role of dispersion and charge transfer energies. The ionization potential of Au_2 is larger in comparison with the ionization potential of Ag_2 but smaller in the case of gold atoms. At the energy minimum the charge transfer from coronene to Au_2 is larger (0.044) than that to Ag_2 (0.042), but the difference is very small and both charge transfers are comparable. When, however, the same distance between coronene and X_2 (X = Ag, Au) is considered, the charge transfer to Ag_2 is larger. This finding agrees with experimental results. It is worth mentioning that a gold atom bound on the coronene surface is characterized by a larger charge transfer[29] than gold dimer. The preferred binding sites of the gold dimer are those that allow double charge transfer. The gold dimer is characterized by higher IP and polarizability than the silver dimer, and this results in a larger dispersion energy between the surface and metal dimer. Because of higher charge transfer and larger dispersion energy, the coronene···Au_2 complexes are about 40% more stable than coronene···Ag_2 complexes.

Whereas Ag_2 and Au_2 bind to coronene surfaces through dispersion and charge-transfer interactions, the much larger binding energies of Pd_2 (about 35 ± 4 kcal/mol) and considerably shorter intermolecular distances (2.06 ± 0.06 Å) evident in Table 3 suggest the presence of a covalent bond. The most stable structure (structure 7) is characterized by two interaction sites, the bridge···top and hollow···top. The binding energies of the other structures are smaller by about 4 kcal/mol. The M06-2X binding energies are about one-third smaller, and the M06-2X intermolecular distances are approximately 0.4 Å longer than the corresponding MP2 results, but the most stable structures are identical.

The Pd atoms in complexes with coronene possess a positive charge (0.05 e), but the detailed analysis indicates two different charge transfer mechanisms. The first involves charge transfer from Pd d-orbitals to coronene and results in a net positive charge on the Pd atoms. The second is a strong interaction involving charge transfer from negatively charged coronene to the positively charged Pd atoms, whereby the lowest unoccupied 5s orbitals of Pd atoms gain a net charge of about 0.1 e. This type of covalent bond is known as a dative bond, and it is responsible for the strong adsorption of the Pd dimer at the carbon surface. It should be stressed that there is no indication of "dative" bond formation in the case of coronene···X_2 (X = Ag, Au) complexes. There is only a one way charge transfer (from coronene to Ag_2 or Au_2), and the backward charge transfer, important in the case of coronene···Pd_2, is missing.

Although the M06-2X method underestimates the binding energies between coronene and metallic dimers, it provides useful information on the behavior of these complexes in both vacuum and water (continuous) environments. The presence of water affects the binding between palladium dimer and coronene only marginally because the differences in binding energies and intermolecular distances in vacuum or water are very small (Table 3). The effect of water on the binding of silver and gold dimers to the coronene surface (Tables 4 and 5) is larger (but not dramatically), with the results showing it decreases charge transfer from coronene to these dimers. Stabilization energies for these dimers are systematically smaller in water (on average by 0.7 and 0.3 kcal/mol for Ag_2 and Au_2, respectively), while intermolecular distances are larger (on average by 0.1 Å). A negligible or small effect of water on the binding of metallic dimers to carbon surfaces is understandable because neither of the interacting partners is charged nor polar.

X_4. Two structures of metallic tetramers were considered (Figure 2): planar square, where all atoms are equivalent, and planar orthorhombic, which has two nonequivalent pairs of atoms, where one pair of diagonal atoms binds to two atoms and the other pair to three atoms. Both structures of the palladium tetramer correspond to a singlet state, which is more

dx.doi.org/10.1021/jp3030733 | J. Phys. Chem. C 2012, 116, 14151−14162

Table 7. Binding Energies (ΔE in kcal/mol) and Intermolecular Distances (R in Å) for the Structures of Graphene···X_2 Complexes[a]

	Pd_2···graphene				Ag_2···graphene				Au_2···graphene			
	1	2	3	4	1	2	3	4	1	2	3	4
PBE/PW												
ΔE	32.1	31.2	29.4	26.0	0.8	0.8	0.8	0.8	1.0	0.9	0.9	0.9
R	2.14	2.12	2.11	2.09	4.00	4.04	4.03	4.05	3.81	3.81	3.82	3.83
PBE+vdW/PW												
ΔE	24.9	24.0	23.2	19.8	5.4	5.7	5.8	5.9	6.7	6.9	7.1	7.1
R	2.27	2.23	2.25	2.26	3.53	3.61	3.59	3.59	3.54	3.52	3.44	3.48
EE+vdW/PW												
ΔE	43.1	38.9	40.9	41.4	5.6	5.7	5.8	5.8	7.0	7.4	7.6	7.7
R	2.26	2.24	2.23	2.25	3.56	3.55	3.56	3.58	3.42	3.43	3.40	3.42

[a]The structures correspond to structures 1, 2, 3, and 4 depicted in Figure 1, but the carbon surface used was graphene.

stable than the triplet state. The most stable structure of Pd_4 is the singlet orthorhombic. The triplet orthorhombic, and singlet and triplet square structures are, respectively, 0.46, 9.92, and 10.15 kcal/mol higher in energy (CASSCF). At the MRSDCI + Q level, the equivalent values are 2.54, 10.61, and 12.22 kcal/mol, respectively.[60] The orthorhombic singlet state is also the most stable for Ag_4 and Au_4. The triplet orthorhombic, and triplet and singlet square structures of Ag_4 are higher in energy by 18.82, 18.96, and 30.64 kcal/mol, respectively (the CCSD(T) level). The order is different for the gold tetramer; the triplet square, triplet orthorhombic, and singlet square are higher by 22.72, 23.59, and 33.24 kcal/mol, respectively (CCSD(T) level). The relative stabilities of the gold tetramer structures agree with those obtained by the CASSCF and POLCI methods.[35]

Although the square structures of silver and gold tetramers are more stable in the triplet than the singlet state, the calculations performed in the present study only concern singlet states. The bond lengths in orthorhombic and planar square structures for singlet states of Pd, Ag, and Au tetramers are 2.512 Å (Pd), 2.683 Å (Ag), 2.639 Å (Au) and 2.681 Å (Pd), 2.664 Å (Ag), 2.610 Å (Au), respectively. The different character of bonding of each structure influences the stability and nature of bonding in the coronene···X_4 complexes.

X_4···Coronene. Binding energies and intermolecular distances of metallic tetramers with coronene are summarized in Table 6. Considering palladium complexes first, the MP2 binding energies for structures 1 and 2 are very large (70.7 and 72 kcal/mol, respectively), much larger than the equivalent values for structures 3 and 4 (39.1 and 44.6 kcal/mol, respectively). The intermolecular distances are rather short and similar to those of coronene···Pd_2 with values of about 2.1 Å. The M06-2X method underestimates the binding energies by more than 20 kcal/mol and overestimates the bond lengths by more than 0.4 (structures 1 and 2) or 0.9 Å (structures 3 and 4).

The binding between Pd_4 and coronene is mediated by a dative bond. The higher stability of structure 2 in comparison with structure 1 is due to larger charge transfer from Pd 4d orbitals to coronene and reverse charge transfer from coronene to Pd 5s orbitals. These two charge transfers are smaller for structure 1, which explains its lower stability.

Binding of structures 3 and 4 was expected to be significantly different from that of structures 1 and 2 because their rhombohedral symmetry leads to different bonding between the metal atoms. Binding energies of the former structures are approximately 40% lower than those of structures 1 and 2 due to lower charge transfer. In structures 3 and 4, two metal atoms in the tetramer undergo significant charge transfer from Pd to coronene as well as charge transfer in the opposite direction. However, the other two tetramer atoms undergo lower charge transfer, and thus the net charge transfer from palladium tetramers to coronene for structures 3 and 4 is less than for structures 1 and 2.

The M06-2X method yields smaller binding energies and larger intermolecular distances than does the benchmark MP2 method. The all electron basis set produces a larger difference in stabilization energy (25−30 kcal/mol) and smaller difference in intermolecular distance (0.5−0.9 Å) than the lanl2dz effective core potential basis set (15−25 kcal/mol and 0.5−1.1 Å, respectively).

The main components of the binding energies of coronene with silver and gold tetramers are dispersion and charge transfer energies, as is the case for complexes of coronene with the respective dimers. The MP2 binding energies of Ag_4···coronene and Au_4···coronene complexes (structures 1, 2, 3, 4) are 14.0, 18.2, 16.5, and 16.2 kcal/mol, and 18.5, 25.0, 23.7, and 23.4 kcal/mol, respectively, which are considerably smaller than the energies of the corresponding palladium complexes. The higher stability of Au_4···coronene complexes as compared to the equivalent Ag_4···coronene complexes is due to a larger charge transfer from coronene to the metallic tetramer, resulting in shorter intermolecular distances. The M06-2X method systematically underestimates the binding energies of the studied complexes. The bond lengths of Ag_4···coronene obtained with the M06-2X method are close to the MP2 values, differing only by about 0.1 Å. However, the relative stabilities are significantly different from those suggested by the MP2 method. In contrast, the M06-2X relative stabilities of Au_4···coronene structures are the same as for the MP2 method, but the M06-2X bond lengths are about 0.2 Å larger.

Structure 2 was found to be the most stable for all of the tetramer metal···coronene complexes. The large stability of this structure can be explained by the presence of significant charge transfer stabilization (double top···top and bridge···top type interaction). Stabilization energies of structures 3 and 4 are comparable but are smaller by about 1.5 kcal/mol than those of structure 2. Structure 1 characterized by a bridge···top interaction is the least stable.

The presence of water decreases the binding energy in Pd_4···coronene complexes by about 10 kcal/mol for structures 1 and 2, and 1 kcal/mol for structures 3 and 4. The binding in this complex is mediated by direct and reverse charge transfer between Pd_4 and coronene. The presence of water reduces the

dx.doi.org/10.1021/jp3030733 | J. Phys. Chem. C 2012, 116, 14151−14162

Table 8. Binding Energies (ΔE in kcal/mol) and Bond Lengths (R in Å) for Different Structures of Coronene···X_4 (X = Pd, Ag, Au) Complexes[a]

	Pd_4···graphene				Ag_4···graphene		Au_4···graphene				
	S1	S2	R3	R4	R1	R2	S1	Y1	Y2	R1	R2
PBE/PW											
ΔE	1.4	1.4	1.6	1.4	1.1	1.1	2.0	1.4	1.4	1.2	1.2
R	3.92	3.93	3.81	3.91	4.11	4.12	3.97	4.01	4.03	4.11	4.08
PBE+vdW/PW											
ΔE	9.7	9.8	10.2	9.8	9.5	9.4	11.9	11.3	11.3	11.2	11.1
R	3.61	3.62	3.58	3.64	3.65	3.67	3.67	3.67	3.67	3.67	3.68
EE+vdW/PW											
ΔE	10.0	9.9	10.6	9.9	9.7	9.5	11.1	11.4	11.3	11.5	11.4
R	3.59	3.62	3.63	3.63	3.66	3.64	3.69	3.56	3.57	3.56	3.58

[a]The letters S, R, and Y denote square, rhombohedral, and Y-shape structures of the tetramer, respectively. S1 and S2 refer to structures 1 and 2 in Table 6, and R1 and R2 refer to structures 3 and 4 in Table 6.

charge transfer, and, consequently, the respective dative bond as well as total binding strength of the complex is weaker. In contrast, water has less of an effect on silver and gold complexes; the binding energy of the most stable structure (structure 1) is slightly increased as compared to in vacuum, whereas it is slightly decreased for the other structures. The reduced effects of water for the gold and silver complexes can be explained by the lower contribution of the charge transfer energy in stabilizing these complexes (dispersion energy is affected by the water considerably less than charge-transfer and mainly electrostatic energy components).

X_2 and X_4···Graphene. Table 7 summarizes the interaction energies for the graphene···metal dimer complexes. We used the same set of positions for all three metals, to provide direct comparison. Because the calculations are computationally demanding, we restricted the number of positions as compared to coronene complexes. The energy differences among various graphene structures are at the DFT level very small (see later), which justify our restriction. We considered the first four structures shown in Figure 1 as well as those in Figure 2. We also restricted the calculations to singlet spin states and geometries obtained at the CCSD(T) level, to facilitate the comparison. Comparing first the binding energies of the graphene···Au_2 and Ag_2 complexes, it is clear that their bonding is very similar. The dominant contribution is due to the van der Waals term, similar to the bonding of Au and Ag atoms on graphene.[29] However, the binding energy calculated using the GGA/PBE approximation is now even lower (~0.4 kcal/mol per atom) because the electrons that are unpaired in atoms can now form bonds with other Au(Ag) atom in the dimer. The PBE+vdW and EE+vdW methods give rather similar binding energies, indicating that the exchange energy of the dimers is well described by the PBE approximation. The binding energies are independent of the position of dimer on the graphene surface, with binding of the Au dimer being slightly stronger due to the larger polarization of gold atoms. Charge transfer between graphene and Au dimer, which significantly contributes to the binding energy at the MP2 level (see former sections), is negligible at the DFT level. The binding energies are consistently slightly lower than the corresponding MP2 values for the coronene···Au_2 and Ag_2 complexes, but agree well with the M06-2X values.

Similar findings can be concluded from the results for graphene···Au_4 and Ag_4 complexes summarized in Table 8. The dominant part of the bonding energy arises from the vdW term, and the binding energies are somewhat lower than their MP2 counterparts. In the case of Au_4 complex, we also considered the Y-shape geometry of the tetramer, which can closely match the positions of carbon atoms in graphene (Figure 3) and has a

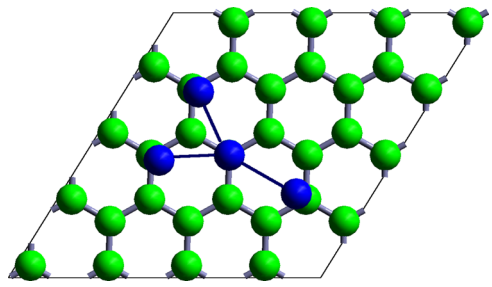

Figure 3. The Y-shape geometry of Au_4 adsorbed on graphene.

dissociation energy (142.2 kcal/mol) just slightly lower than that of the most favorable rhombohedral structure (143.0 kcal/mol). According to the results shown in Table 8, both geometries are also very close in terms of the binding energy to the graphene surface. For Ag_4, we only considered the rhombohedral geometry because the square geometry is energetically unfavorable.

In general, the equilibrium distances for Au and Ag dimers and tetramers are longer than those of the respective graphene···atom complexes, mainly because of the greater exchange repulsion between the dimer and carbon atoms in the graphene sheet. An analogous elongation was observed for coronene complexes, both at the MP2 and at the M06-2X levels. The incorporation of exact exchange reduces the bonding distances for atom···graphene complexes.[29] However, this effect is less pronounced for clusters. The distances of the metal atom−carbon bonds increase in the order benzene < coronene < graphene, but no such trend is evident for clusters; the distances for different arenes are rather consistent.

On examining the binding energies of the graphene···Pd_2 and Pd_4, one finds a striking feature: while the Pd dimer binds strongly to the graphene surface, analogous to the covalently bound Pd atom,[29] the binding of the Pd tetramer appears to be similar to the binding of Au and Ag clusters; the bonding is rather weak, the dominant contribution comes from the van der Waals term, and PBE gives only negligible bonding. This character of bonding of Pd_4 is thus in stark contrast to the results presented in the previous section, because both MP2 and M06-2X predict stronger binding of Pd_4 in comparison with Pd_2. There appears to be no simple explanation of this

dx.doi.org/10.1021/jp3030733 | J. Phys. Chem. C 2012, 116, 14151−14162

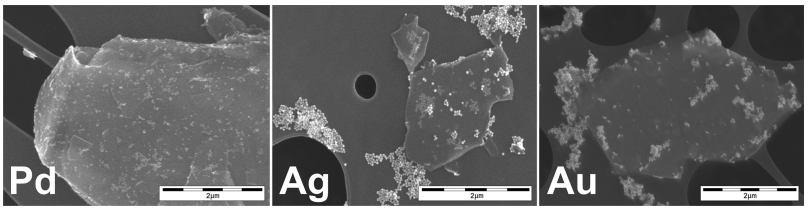

Figure 4. SEM images of graphene−Pd (left), graphene−Ag (middle), and graphene−Au (right) composites.

disagreement; the difference between graphene and coronene is not likely to be the reason. One explanation may be the delicate balance between the energy penalty associated with weakening the Pd−Pd bonds inside Pd clusters and the energy gained by creating new bonds with carbon atoms. Pd atoms are bound strongly in the tetramer, which is reflected in its high dissociation energy. At the DFT PBE level, the dissociation energy per atom of Pd_4 is 38.4 kcal/mol, whereas only 11.2 kcal/mol is needed to dissociate singlet Pd dimer. Thus, the electron density in the dimer is probably more easily relocalized to overlap with one of the carbon atoms, whereas such a change would be less favorable in the tetramer. If the methods calculate this energy balance differently, they may converge to completely different final states.

Comparison of Binding Energies of Coronene and Graphene Complexes. The MP2 results of binding energies represent benchmark data for the studied coronene complexes. Although MP2 tends to slightly exaggerate the binding energies, both exchange and long-range correlations are treated more consistently in this method than in the DFT method, which was utilized for graphene···X clusters. Comparing the binding energies for the most favorable structure of coronene···X, coronene···X_2, and coronene···X_4, we identified an almost linear dependence on the number of metal atoms. In the case of palladium, silver, and gold, we obtained the following ratios: 1:2.2:4; 1:2.2:4.4; 1:1.85:3.6. We can thus conclude that the binding energy of the metal clusters increases linearly with the number of metal atoms, and similar results were obtained for all of the studied metals. This result is rather surprising considering the different nature of binding of Pd, Ag, and Au clusters. Further, this trend was not observed for graphene···X, graphene···X_2, and graphene···X_4 complexes; a linear dependence of binding energy was confirmed for silver and gold complexes but not for palladium complexes.

It should be remembered that binding of Pd clusters on carbon surfaces is mediated by a dative bond. Therefore, one explanation for this difference is based on the structure of palladium clusters. The linear dependence of the binding energies of Pd clusters on coronene was obtained under the assumption that the energetically most stable structure of the coronene···Pd_4 complex was considered. As mentioned above, in this structure, all Pd atoms are equivalent and all Pd···Pd distances are equal. When the energetically less stable structures 3 and 4 of the coronene···Pd_4 complex were considered, the above-mentioned ratio changed as follows: 1:2.2:2.5; 1:2.2:4; 1:1.85:3.4. For these structures, the binding energy of Pd_4 is now similar to that of Pd_2, and this result agrees with those for graphene···X complexes. The Pd atoms in structure 3 and 4 are nonequivalent; some of the atoms are bound to only two metal atoms, whereas others are bound to three neighbors. Hence, an alternative explanation for the lack of linear dependence of the binding energy on the number of Pd atoms is that the Pd atoms in these structures are more saturated by the bonding between them, and thus have a lower affinity to form bonds with surface atoms. A similar rationale may explain the binding energies of Pd clusters on graphene.

In summary, considering the most stable structures, our results suggest that the binding energy between Pd, Au, and Ag clusters and coronene increases linearly with the number of noble metal atoms. On the other hand, the binding energy has to become saturated for large clusters, because the studies of semi-infinite graphene−noble metal interfaces show rather similar bonding properties.[15] Our results suggest that the interaction of small clusters displays a higher variety in bonding properties, which may arise from size effects and specific atomic coordination. The binding of Pd is considerably stronger than that of Au complexes, which in turn is slightly stronger than the binding of Ag complexes. This conclusion is based on the most reliable DK-MP2 calculations employing a large basis set.

Affinity of Metal Nanoparticles to Graphene. We prepared composites of graphene with metal (Ag, Au, and Pd) nanoparticles (~20 nm) to qualitatively compare the results of the theoretical calculations with the experimentally determined affinity between graphene and the respective metal nanoparticles. SEM images of the coated surface (Figure 4) demonstrated that the graphene sheets were homogeneously covered with Pd nanoparticles. We did not observe any Pd nanoparticles or their agglomerates outside of the graphene sheets. This is consistent with the high calculated interaction energy of Pd to graphene, whereas the mutual interaction among Pd nanoparticles is limited, as indicated by the absence of metal aggregates. In contrast, SEM images of Ag−graphene and Au−graphene nanocomposites revealed a completely different character of interaction as evidenced by the presence of a large number of silver (gold) aggregates covering not only the graphene surface but also projecting out of the graphene sheets. This behavior is suggestive of a lower interaction energy between silver (gold) nanoparticles and graphene and a higher tendency to agglomerate with respect to palladium.

CONCLUSIONS

(i) The MP2 method combined with the ANO-RCC-VDZP basis set provides reliable stabilization energies and intermolecular distances comparable to CCSD(T) values for benzene···Pd_2 and benzene···Ag_2 complexes. In the case of gold complexes, the MP2 stabilization energies are about 50% larger than for Ag_2 and Pd_2 complexes.

(ii) M06-2X stabilization energies are systematically smaller than the equivalent MP2 values, whereas the respective intermolecular distances are systematically larger. The stability order in the Pd−Au−Ag series is retained.

(iii) Palladium complexes (dimers as well as tetramers) are considerably stronger bonded to coronene than gold and silver complexes. Pd_2 interacts with the coronene surface through a dative bond, which is mediated by charge transfer from the metallic dimer to the coronene surface

dx.doi.org/10.1021/jp3030733 | J. Phys. Chem. C 2012, 116, 14151−14162

and reverse charge transfer from coronene to the positively charged Pd_2. The chemisorption of Pd_4 on coronene surface is characterized by the same bonding.

(iv) Silver and gold dimers are bound to coronene surface by dispersion and charge transfer interactions. The latter in particular plays an important role, with the most stable structures being characterized by double charge transfer from coronene to the metal dimer. The complexes of gold dimer are more stable than those of silver due to the higher electron affinity of Au_2, which results in greater charge transfer from coronene to the metal dimer. The nature of bonding in coronene···X_4 complexes is similar to that in coronene···X_2. Ag and Au tetramers prefer structures characterized by direct top···top and bridge···top interactions, which is due to a large amount of charge transfer.

(v) MP2 calculations on coronene···X complexes indicate that binding of Pd, Ag, and Au clusters increases linearly with the number of metallic atoms. This finding was also observed for graphene···X complexes with the exception of graphene···Pd_4 complexes, where the binding energy is comparable to that of graphene···Pd_2. We believe that the MP2 results are reliable, and it is difficult to explain the failure of the DFT calculations.

(vi) Charge transfer from coronene to dimers and tetramers of Pd, Ag, and Au is reduced in water. This leads to increased bond lengths and destabilization of the bond between metal clusters and coronene, but these differences are modest (less than about 20%). The moderate effect of water can be understood on the basis of the fact that the interacting subsystems (coronene, metal dimers, and tetramers) are all electro-neutral and nonpolar.

(vii) On the basis of MP2 calculations, we conclude that the stability of metal clusters (up to tetramers) on coronene increases as follows: Pd ≫ Au > Ag.

(viii) SEM images of graphene composites with metal nanoparticles (∼20 nm) suggest that the affinity of Pd nanoparticles to graphene is significantly higher than the affinity of Ag (Au) nanoparticles in agreement with MP2 theoretical calculations.

AUTHOR INFORMATION

Corresponding Author

*Tel.: +420 585 634 756 (M.O.); +420 220 410 311 (P.H.). Fax: +420 585 634 761 (M.O.); +420 220 410 320 (P.H.). E-mail: michal.otyepka@upol.cz (M.O.); pavel.hobza@marge.uochb.cas.cz (P.H.).

Author Contributions

§These authors contributed equally to this work.

Notes

The authors declare no competing financial interest.

ACKNOWLEDGMENTS

This work was supported by the Grant Agency of the Czech Republic [P208/12/G016 and P208/10/1742]. This work was also supported by the Operational Program Research and Development for Innovations − European Regional Development Fund (CZ.1.05/2.1.00/03.0058) and European Social Fund (CZ.1.07/2.3.00/20.0017). This work was also supported by NRF (WCU: R32-2008-000-10180-0). The support of Praemium Academiae of the Academy of Sciences of the Czech Republic awarded to P.H. in 2007 is also acknowledged.

REFERENCES

(1) Novoselov, K. S.; Geim, A. K.; Morozov, S. V.; Jiang, D.; Zhang, Y.; Dubonos, S. V.; Grigorieva, I. V.; Firsov, A. A. *Science* **2004**, *306*, 666−669.

(2) Geim, A. K.; Novoselov, K. S. *Nat. Mater.* **2007**, *6*, 183−191.

(3) Zhang, Y. B.; Tan, Y. W.; Stormer, H. L.; Kim, P. *Nature* **2005**, *438*, 201−204.

(4) Zhang, Y.; Jiang, Z.; Small, J. P.; Purewal, M. S.; Tan, Y. W.; Fazlollahi, M.; Chudow, J. D.; Jaszczak, J. A.; Stormer, H. L.; Kim, P. *Phys. Rev. Lett.* **2006**, *96*, 136806.

(5) Areshkin, D. A.; Gunlycke, D.; White, C. T. *Nano Lett.* **2007**, *7*, 204−210.

(6) Tombros, N.; Jozsa, C.; Popinciuc, M.; Jonkman, H. T.; van Wees, B. J. *Nature* **2007**, *448*, 571−574.

(7) Sundaram, R. S.; Steiner, M.; Chiu, H.-Y.; Engel, M.; Bol, A. A.; Krupke, R.; Burghard, M.; Kern, K.; Avouris, P. *Nano Lett.* **2011**, *11*, 3833−3837.

(8) Baby, T. T.; Aravind, S. S. J.; Arockiadoss, T.; Rakhi, R. B.; Ramaprabhu, S. *Sens. Actuators, B* **2010**, *145*, 71−77.

(9) Hong, W. J.; Bai, H.; Xu, Y. X.; Yao, Z. Y.; Gu, Z. Z.; Shi, G. Q. *J. Phys. Chem. C* **2010**, *114*, 1822−1826.

(10) Li, Y.; Fan, X. B.; Qi, J. J.; Ji, J. Y.; Wang, S. L.; Zhang, G. L.; Zhang, F. B. *Mater. Res. Bull.* **2010**, *45*, 1413−1418.

(11) Li, Y.; Fan, X. B.; Qi, J. J.; Ji, J. Y.; Wang, S. L.; Zhang, G. L.; Zhang, F. B. *Nano Res.* **2010**, *3*, 429−437.

(12) Scheuermann, G. M.; Rumi, L.; Steurer, P.; Bannwarth, W.; Mulhaupt, R. *J. Am. Chem. Soc.* **2009**, *131*, 8262−8270.

(13) Shan, C. S.; Yang, H. F.; Han, D. X.; Zhang, Q. X.; Ivaska, A.; Niu, L. *Biosens. Bioelectron.* **2010**, *25*, 1070−1074.

(14) Xiong, Z. G.; Zhang, L. L.; Ma, J. Z.; Zhao, X. S. *Chem. Commun.* **2010**, *46*, 6099−6101.

(15) Giovannetti, G.; Khomyakov, P. A.; Brocks, G.; Karpan, V. M.; van den Brink, J.; Kelly, P. J. *Phys. Rev. Lett.* **2008**, *101*, 206803.

(16) Khomyakov, P. A.; Giovannetti, G.; Rusu, P. C.; Brocks, G.; van den Brink, J.; Kelly, P. J. *Phys. Rev. B* **2009**, *79*, 195425.

(17) Varykhalov, A.; Scholz, M. R.; Kim, T. K.; Rader, O. *Phys. Rev. B* **2010**, *82*, 121101.

(18) Jensen, P.; Blase, X.; Ordejon, P. *Surf. Sci.* **2004**, *564*, 173−178.

(19) Wang, G. M.; BelBruno, J. J.; Kenny, S. D.; Smith, R. *Phys. Rev. B* **2004**, *69*, 195412-1−195412-7.

(20) Varns, R.; Strange, P. *J. Phys.: Condens. Matter* **2008**, *20*, 225005.

(21) Akola, J.; Hakkinen, H. *Phys. Rev. B* **2006**, *74*, 165404-1−165404-9.

(22) Amft, M.; Sanyal, B.; Eriksson, O.; Skorodumova, N. V. *J. Phys.: Condens. Matter* **2011**, *23*, 205301.

(23) Chan, K. T.; Neaton, J. B.; Cohen, M. L. *Phys. Rev. B* **2008**, *77*, 235430-1−235430-12.

(24) Jalkanen, J. P.; Halonen, M.; Fernandez-Torre, D.; Laasonen, K.; Halonen, L. *J. Phys. Chem. A* **2007**, *111*, 12317−12326.

(25) Thapa, R.; Sen, D.; Mitra, M. K.; Chattopadhyay, K. K. *Physica B* **2011**, *406*, 368−373.

(26) Grimme, S. *WIREs Comput. Mol. Sci.* **2011**, *1*, 211−228.

(27) Cohen, A. J.; Mori-Sánchez, P.; Yang, W. T. *Chem. Rev.* **2012**, *112*, 289−320.

(28) Amft, M.; Lebegue, S.; Eriksson, O.; Skorodumova, N. V. *J. Phys.: Condens. Matter* **2011**, *23*, 395001.

(29) Granatier, J.; Lazar, P.; Otyepka, M.; Hobza, P. *J. Chem. Theory Comput.* **2011**, *7*, 3743−3755.

(30) Neogrády, P.; Urban, M.; Hubač, I. In *Recent Advances in Clouped-Cluster Methods*; Bartlett, R. J., Ed.; World Scientific: Singapore, 1997; p 275.

(31) Neogrády, P.; Urban, M. *Int. J. Quantum Chem.* **1995**, *55*, 187−203.

(32) Watts, J. D.; Gauss, J.; Bartlett, R. J. *J. Chem. Phys.* **1993**, *98*, 8718−8733.

(33) Li, S. G.; Hennigan, J. M.; Dixon, D. A.; Peterson, K. A. *J. Phys. Chem. A* **2009**, *113*, 7861−7877.

(34) Tekarli, S. M.; Drummond, M. L.; Williams, T. G.; Cundari, T. R.; Wilson, A. K. *J. Phys. Chem. A* **2009**, *113*, 8607−8614.

(35) Balasubramanian, K.; Feng, P. Y.; Liao, M. Z. *J. Chem. Phys.* **1989**, *91*, 3561−3570.
(36) Möller, C.; Plesset, M. S. *Phys. Rev.* **1934**, *46*, 0618−0622.
(37) Zhao, Y.; Truhlar, D. G. *J. Chem. Phys.* **2006**, *125*, 194101.
(38) Zhao, Y.; Truhlar, D. G. *J. Chem. Theory Comput.* **2007**, *3*, 289−300.
(39) Zhao, Y.; Truhlar, D. G. *Theor. Chem. Acc.* **2008**, *120*, 215−241.
(40) Roos, B. O.; Lindh, R.; Malmqvist, P. A.; Veryazov, V.; Widmark, P. O. *J. Phys. Chem. A* **2004**, *108*, 2851−2858.
(41) Roos, B. O.; Lindh, R.; Malmqvist, P. A.; Veryazov, V.; Widmark, P. O. *J. Phys. Chem. A* **2005**, *109*, 6575−6579.
(42) Douglas, M.; Kroll, N. M. *Ann. Phys.* **1974**, *82*, 89−155.
(43) Hess, B. A.; Chandra, P. *Phys. Scr.* **1987**, *36*, 412−415.
(44) Boys, S. F.; Bernardi, F. *Mol. Phys.* **1970**, *19*, 553−566.
(45) Hay, P. J.; Wadt, W. R. *J. Chem. Phys.* **1985**, *82*, 270−283.
(46) Hay, P. J.; Wadt, W. R. *J. Chem. Phys.* **1985**, *82*, 299−310.
(47) Marenich, A. V.; Cramer, C. J.; Truhlar, D. G. *J. Phys. Chem. B* **2009**, *113*, 6378−6396.
(48) Koch, H.; de Meras, A. S.; Pedersen, T. B. *J. Chem. Phys.* **2003**, *118*, 9481−9484.
(49) Karlstrom, G.; Lindh, R.; Malmqvist, P. A.; Roos, B. O.; Ryde, U.; Veryazov, V.; Widmark, P. O.; Cossi, M.; Schimmelpfennig, B.; Neogrady, P.; et al. *Comput. Mater. Sci.* **2003**, *28*, 222−239.
(50) Frish, M. J.; Trucks, G. W.; Schlegel, H. B.; Scuseria, G. E.; Robb, M. A.; Cheesman, J. R.; Scalmani, G.; Barone, V.; Mennucci, B.; Petersson, G. A.; et al. *Gaussian 09*, revision A.02; Gaussian, Inc.: Wallingford, CT, 2009.
(51) Blochl, P. E. *Phys. Rev. B* **1994**, *50*, 17953−17979.
(52) Kresse, G.; Joubert, D. *Phys. Rev. B* **1999**, *59*, 1758−1775.
(53) Perdew, J. P.; Burke, K.; Ernzerhof, M. *Phys. Rev. Lett.* **1996**, *77*, 3865−3868.
(54) Dion, M.; Rydberg, H.; Schroder, E.; Langreth, D. C.; Lundqvist, B. I. *Phys. Rev. Lett.* **2005**, *95*, 109902.
(55) Lazic, P.; Atodiresei, N.; Alaei, M.; Caciuc, V.; Blugel, S.; Brako, R. *Comput. Phys. Commun.* **2010**, *181*, 371−379.
(56) Panáček, A.; Kvítek, L.; Prucek, R.; Kolář, M.; Večeřová, R.; Pizúrová, N.; Sharma, V. K.; Nevěčná, T.; Zbořil, R. *J. Phys. Chem. B* **2006**, *110*, 16248−16253.
(57) Andreescu, D.; Sau, T. K.; Goia, D. V. *J. Colloid Interface Sci.* **2006**, *298*, 742−751.
(58) Balasubramanian, K. *J. Chem. Phys.* **1988**, *89*, 6310−6315.
(59) Seminario, J. M.; Zacarias, A. G.; Castro, M. *Int. J. Quantum Chem.* **1997**, *61*, 515−523.
(60) Dai, D. G.; Balasubramanian, K. *J. Chem. Phys.* **1995**, *103*, 648−655.
(61) Černušák, I.; Diercksen, G. H. F.; Sadlej, A. J. *Phys. Rev. A* **1986**, 33, 814−823.